RSC Advances

ROYAL SOCIETY OF CHEMISTRY

www.rsc.org/advances

Mechanical Properties of High-performance Elastomeric Nanocomposites: A Sequential Mesoscale Approach

Deng Shengwei,[a] Huang Yongmin,[a] Xu Shouhong,[a] Lin Shaoliang,[b] Liu Honglai,[*a] Hu Ying[a]

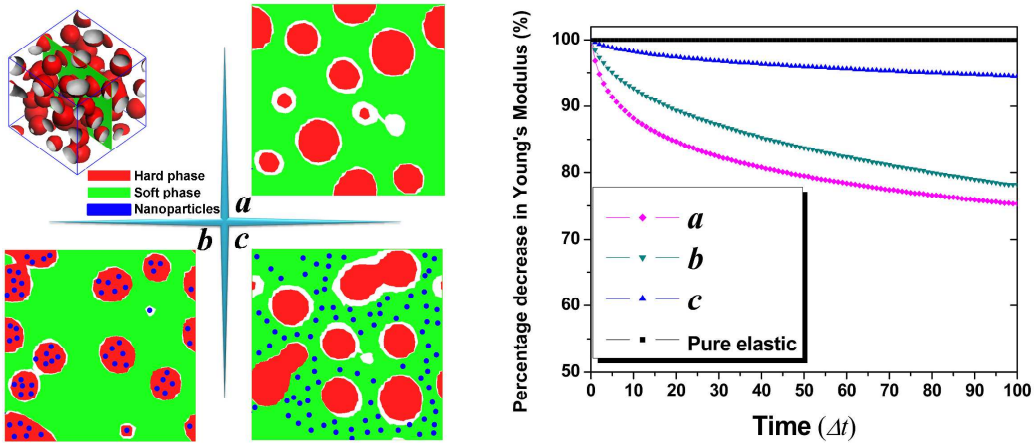

A sequential mesoscale simulation method was adopted to formulate elastomeric nanocomposites with desired macroscopic mechanical responses

Mechanical Properties of High-performance Elastomeric Nanocomposites: A Sequential Mesoscale Simulation Approach

Deng Shengwei,[a] Huang Yongmin,[a] Xu Shouhong,[a] Lin Shaoliang,[b] Liu Honglai,[*a] Hu Ying[a]

The incorporation of nanoparticles into elastomeric block copolymers affords engineers an opportunity to obtain polymer nanocomposites that potentially rival the most advanced materials in nature. A computationally efficient simulation method that utilized MesoDyn for morphologies and lattice spring model (LSM) for mechanical properties was adopted in this work. Simulation results show that the selective distribution of nanoparticles in hard or soft segment microdomains of block copolymers will narrow the phase domain size in bicontinuous structures. The Zener model was incorporated into pure elastic LSM to capture the stress relaxation behavior. Mechanical tests reveal that the stress transfer between the polymer matrix and nanoparticles in different composites is critical to the stiffness enhancement. In dispersed structures, adding nanoparticles in hard microdomain can increase the elastic modulus and maintain high extensibility without impairing its viscosity dramatically. The methods developed in this work yield guidelines for formulating elastomeric nanocomposites with desired macroscopic mechanical responses.

Introduction

Polymer nanocomposites are of widely scientific and commercial interests due to the enhanced properties compared to neat polymers[1-6]. Normally, appropriately adding nanoparticles to a polymer matrix can enhance its performance, e.g., high aspect-ratio nanofillers with well-dispersion or exfoliation in polymer result in extremely high stiffness[7, 8]. However, these additives with homogeneous distribution in polymer matrix may also have adverse effects. These nanocomposites are usually stiff but inextensible, like ceramic, or extensible but soft, like rubber[9]. Selectively reinforcing certain domains of phase-separated block copolymers with inorganic nanoparticles would be a proper way to achieve unprecedented improvements in stiffness and strength without losses in the extensibility of the composites[10, 11]. Gareth and co-workers[12] used a two-solvent processing approach to obtain the high-performance material based on hard-soft block copolymers (Elasthane). The nanofillers distributed in the hard phase gave rise to a dramatic increase in stiffness of up to 23-fold and a concurrent improvement in strength, while the extensibility was maintained which was determined by unreinforced soft phase.

Inspired by high-performance Elasthane nanocomposites, hard-soft block copolymers with bicontinuous and dispersed structures are utilized as model systems, and nanoparticles are dispersed into the hard phase, soft phase or interface by varying the interaction between the nanoparticle and polymer. Thermodynamic or kinetic barriers may inhibit the selective dispersal of nanoparticles in polymer matrices, e.g. hydrophilic nanoparticles in hydrophobic polymer microdomains. Fortunately, recent experiments[12] showed that it is possible to overcome this obstacle by advanced experimental techniques. Comparing with mature experimental techniques, only a few simulation works correlate the structure and mechanical behaviour of this kind of high-performance materials[13]. Due to the complexity of polymer nanocomposites, the main challenge for simulating the mechanical properties is the restriction by the computing capability, and an effective simulation method with wide applicability is favourable. Based on our previous works[14, 15], a computationally efficient method (Sequential mesoscopic simulation) was adopted in this work to capture mechanical responses such as the stiffness, fracture strain and stress relaxation. This method utilized MesoDyn simulation[16-18] for structures and lattice spring model (LSM) for mechanical properties. Subsequently, the pure elastic model was replaced by an anelastic solid model (Zener model) in LSM to study the viscoelastic behavior.

In order to obtain morphologies of different composites, atomic simulations provide the first opportunity in sight to reach the most precise model[19]. In this work, a huge number of nanoparticles should be modelled efficiently, and then the discrete positions of particles inevitably need to be replaced by a cruder description[20, 21]. Field-based approaches are more suitable for obtaining the structure evolution information comparing to atomic simulations which are computationally expensive. Therefore, dynamic density functional theory embodied in MesoDyn was adopted to simulate the meso-structures[22].

LSM is a discretized method for continuum elastic media and often used to simulate deformation and fracture of complicated structural systems. For more details related to LSM, see ref. [23-26]. An important part of this work is the incorporation of linear viscoelastic model into pure elastic LSM. In many cases, elastic constitutive model works well when time dependent effect can be neglected. Otherwise, more appropriate constitutive model is needed to describe the mechanical behavior. Time dependent effect indicates that the stress-strain behavior of materials changes with the time. Monette et al. [27] investigated the mechanical properties of short-fiber polymer

composites by a two-dimensional triangular lattice, which described the viscoelastic behavior through the incorporation of Maxwell units. Buxton et al. [28] studied the viscous deformation of homopolymers containing various shapes of nanofillers by LSM. In this work, a similar approach based on Monette and Buxton's work was adopted to capture the stress relaxation behavior of different multi-component composites, which especially focused on the influence of selective dispersal of nanoparticles on the viscous deformation.

Model and simulation method

The sequential simulation method combines the MesoDyn simulation for nanocomposite morphologies with the pure elastic or viscoelastic LSM for mechanical properties. The output of the former serves as the input of the latter.

A. MesoDyn Simulation

The structural evolution of block copolymer and its nanocomposites was simulated by using the MesoDyn program incorporated in the Materials Studio, version 5.5, from Accelrys. MesoDyn method is based on the dynamic mean-field density functional theory, in which the dynamics of phase separation can be described by Langevin equations to study the diffusion of the density field. There is a one-to-one relationship between the density distribution function of the system and the external potential field. The free energy F of an inhomogeneous liquid is a function of density field ρ(r), and all thermodynamic functions can be derived from the free energy. The polymer chains are modelled as ideal independent Gaussian chains consisting of beads and a mean-field non-ideal contribution. The chain topology depends on the coarsening degree of the original system. On a coarse-grained time scale, a probability Ψ can be assigned to a certain configuration of bead positions, correspondingly, a free energy functional $F[\Psi]$ can be constructed. Taking conditional minimum, the undetermined multiplier U_I is just the external potential, then the density functional of the free energy can be obtained as:

$$\beta F[\rho] = n\ln\Phi + \beta^{-1}\ln n! - \sum_{I}\int U_I(\boldsymbol{r})\rho_I(\boldsymbol{r})\mathrm{d}\boldsymbol{r} + \beta F^{\mathrm{nid}}[\rho] \quad (1)$$

where I stands for different kinds of monomers, β=1/kT, n is the total number of chains, and Φ is the partition function of a single chain. The mean-field nonideal free energy functional F^{nid} with two kinds of monomers is expressed by:

$$F^{\mathrm{nid}}[\rho] = \frac{1}{2}\sum_{I,J}\int\int \in_{IJ}(|\boldsymbol{r}-\boldsymbol{r}'|)\rho_I(\boldsymbol{r})\rho_J(\boldsymbol{r}')\mathrm{d}\boldsymbol{r}\mathrm{d}\boldsymbol{r}' \quad (2)$$

where $\in_{IJ}(|\boldsymbol{r}-\boldsymbol{r}'|)$ is an interaction energy parameter between the bead of type I at $\boldsymbol{r}$ and the one of type J at $\boldsymbol{r}'$.

The intrinsic chemical potentials can be derived by functional differentiation of the free energy, $\mu_I(\boldsymbol{r}) = \delta F / \delta\rho_I(\boldsymbol{r})$.

On the basis of these equations, the generalized time-dependent Ginzburg-Landau theory can be established. The time dependence is described by a diffusion equation. The Langevin equations for the diffusion dynamics of the density fields are then given by:

$$\frac{\partial\rho_A}{\partial t} = Mv_B\nabla\rho_A\rho_B\nabla[\mu_A - \mu_B] + \eta \quad (3)$$

$$\frac{\partial\rho_B}{\partial t} = Mv_B\nabla\rho_A\rho_B\nabla[\mu_B - \mu_A] + \eta \quad (4)$$

where M is a bead mobility parameter. The Gaussian noise η satisfies the fluctuation-dissipation theorem:

$$<\eta(\boldsymbol{r},t)>=0 \quad (5)$$

$$< \eta(\mathbf{r},t)\eta(\mathbf{r}',t') >= -2Mv_B\beta^{-1}\delta(t-t')\nabla\mathbf{r}\cdot\delta(\mathbf{r}-\mathbf{r}')\rho_A\rho_B\nabla\mathbf{r}' \quad (6)$$

The kinetic coefficient $Mv_B\rho_A\rho_B$ models a local exchange mechanism. The Langevin equations are constructed for an incompressible system with dynamic constraints:

$$(\rho_A(\mathbf{r},t)+\rho_B(\mathbf{r},t)) = \frac{1}{v_B} \quad (7)$$

where v_B is an average bead volume.

B. Lattice Spring Model for Simulating Elastic Deformation and fracture

Born LSM is a numerical technique for discretizing the linear elasticity theory, and it is frequently used to simulate deformation and fracture of materials. The material is represented by a network of springs, which occupy the nearest and next nearest neighbour bonds of a simple cubic lattice. Although lack of rotational invariance, in the systems considered here, rotations are assumed to be small, and therefore a Born spring model is implemented. By assigning different force constants according to the composition of different nodes, the model is successful in the study of heterogeneous systems. Typically, the lattice spring model allows us to determine micromechanical properties in a computationally efficient way.

The energy associated with a node m in the cubic lattice is taken to be of the form[23]

$$P_m = \frac{1}{2}\sum_n (\boldsymbol{u}_m - \boldsymbol{u}_n)^{\mathrm{T}} \cdot \boldsymbol{M}_{mn} \cdot (\boldsymbol{u}_m - \boldsymbol{u}_n) \quad (8)$$

where n is the neighboring nodes connected to m by a spring, the vector $\boldsymbol{u}_m$ is the displacement of the mth node from its original position, $\boldsymbol{M}_{nm}$ is a symmetric 3×3 tensor which describes the interaction between various nodes through central and noncentral force constants. The central force constant energetically compensates the spring extension, while the noncentral force constant penalizes the rotation of springs from their original orientation. By mapping of the spring model onto continuum equations, the central force constant k and noncentral force constant c take the following forms,

$$k = \frac{E}{5(1-2\nu)} \qquad c = \frac{E(1-4\nu)}{5(1+\nu)(1-2\nu)} \quad (9)$$

where E and v are the Young's modulus and Poisson's ratio, respectively.

The elastic force acting on the mth node is a linear function of the displacement because of the harmonic form of energy in equation 8. The force acting on the mth node, due to the local displacement of the spring between nodes m and all neighboring n, is given by

$$\boldsymbol{F}_m = \sum_n \boldsymbol{M}_{nm} \cdot (\boldsymbol{u}_m - \boldsymbol{u}_n) \quad (10)$$

If the external forces are applied to the boundary nodes with the spring constants specified, the constraint that all these linear forces must balance at each node at equilibrium results in a set of sparse linear equations. The solution of these equations is obtained by using a conjugate gradient method to find the equilibrium configuration corresponding to the situation without net force at each node. The stress and strain tensors are calculated by the forces and displacements. The average strain and the applied stress can then be used to calculate the Young's modulus (stiffness) which is defined as the stress of a material divided by its strain.

The critical fracture strain is a measure of the extensibility of the material which corresponds to the maximum strain that the system can sustain before happening catastrophic failure. In order to obtain the fracture strain of different polymer materials, here we adopt a

probabilistic method, which indicates that a fracture is considered to be formed with a probability proportional to the local stress. To determine when the fracture surface is to be created, a rate of failure $p_s(t)$ of a surface s at time t is introduced as follows:

$$p_s(t) = \left[\frac{(\sigma_s(t) - e_s)}{e'_s} \right]^{\beta} \quad (11)$$

where is the local stress, e_s is the minimum value of stress at which fracture can occur, and e'_s is an arbitrary scaling parameter (here we choose $e'_s = e_s$). The minimum stress e_s for a fracture between two nodes is simply set to the mean value of the minimum fracture stress of the two nodes. The modulus β allows for a nonlinear relationship between failure rate and stress field (here we choose $\beta = 2$). Actually, the minimum value of stress e_s is closely related to the toughness of materials, and the latter is defined by the area under a stress-strain plot from the beginning to the fracture point. Assuming that a damage occurs somewhere in the system, the probability of failure, $P_s(t)$, occurring at a given surface s is the rate associated with the surface s relative to the total rate of damage occurring throughout the material, i.e., $P_s(t) = p_s(t) / \Sigma_{s'} p_{s'}(t)$, where the sum $\Sigma_{s'}$ is over all surfaces. The surface chosen to fracture is related to this probability. The average time interval for this failure event to occur is

$$\Delta t = \frac{1}{\sum_{s'} p_{s'}(t)} \quad (12)$$

To initiate fracture, a constant strain rate is applied to the sample with periodic boundary condition adopted. The strain is varied in a predetermined range by a golden section method to find the crack tip (the strain error is less than 0.1%). An initial time step Δt_0 is introduced; the fracture occurs if the average time interval is smaller than Δt_0. After the beginning of the fracture, the applied strain rate will be increased at each iteration by a constant (here we choose 0.001). Therefore, the creation of fracture surfaces depends on the correct probability weightings in equation 11, and the relaxation of material surrounding the propagating crack tip takes the average time interval over which the crack grows into consideration. In this manner, the deformation and fracture cease at the fracture point when the stress no longer increases with the increase of strain, and the strain and stress at this point correspond to the fracture strain and tensile strength, respectively. More detailed description about the fracture process can be found in our previous work [14, 29].

C. Viscoelastic LSM for studying stress relaxation

The spring between nodes in LSM was replaced by a viscoelastic model to capture the stress relaxation behaviour of different composites. In pure elastic LSM, the strain applied to the system boundaries increases by a constant at each time step, which enables the system to evolve through a series of equilibrium states. The time step is not related to the real time. In viscoelastic LSM, a time frame is introduced through the incorporation of viscous deformation in each iteration. The equilibrium bond lengths are no longer constant, but time dependent, which incorporates viscous deformations related to the viscosity of different components. Similarly, the plasticity can also be incorporated into LSM, force constants will update in each iteration according to plastic model, while the plastic behaviour is beyond the research scope of this paper.

As shown in Fig. 1, an anelastic solid model (Zener model) is considered in this work to replace the previous pure elastic model. This model consists of a Kelvin unit in series with an elastic unit (spring), and it is often used to describe creep and stress relaxation behaviors.

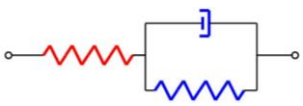

Fig. 1 The anelastic solid model composed of a Kelvin unit (a spring of modulus E in parallel with a dashpot of viscosity η) in series with a spring of modulus E

For simplicity, springs in the model use the same sprint constant, and this treatment is enough to provide a reasonable adjustment range of stress relaxation. The stress can be reduced by half if time approached infinity, the degree of stress relaxation is influenced by the strain rate and viscosity. When a constant uniaxial stress σ_0 is applied to a homogeneous system, the response function is given by:

$$\varepsilon(t) = (\frac{2}{E} - \frac{1}{E}\exp(-t/\tau))\sigma_0 \quad (13)$$

where $\varepsilon(t)$ is the strain at time t, τ represents the relaxation time given by $\tau = \eta/E$, η is the viscosity of corresponding material. The strain is initially σ_0 / E and tends towards $2\sigma_0 / E$ if time approaches infinity. Both the Young's modulus and viscosity are related to the composition of each node, and the above model will be applied in all 18 directions for each node. Note that the time scale here is significantly longer than the dampening of elastic waves, and hence the viscoelastic mechanical process can be treated as a sequence of equilibrium states. The viscous deformations do not vary significantly between iterations. Therefore, the increment in current viscous deformation is calculated from the previous iteration information. Take two neighboring bonds m and n for example, we define that the force applied between these two nodes is $\boldsymbol{F}$ at time t. According to the model in Fig. 1, forces acting on the elastic unit and Kelvin unit are also equal to $\boldsymbol{F}$; displacements of spring and dashpot are the same in Kelvin unit. Then we can obtain the force acting on the dashpot at $t+\Delta t$ based on the viscous displacement at time t.

$$\boldsymbol{F}_{\text{vis}} = \boldsymbol{M}_{mn}\boldsymbol{u}_{mn} - \boldsymbol{M}^{\boldsymbol{v}}_{mn}\boldsymbol{u}^{\boldsymbol{v}}_{mn} = (\boldsymbol{u}^{v}_{mn}(t+\Delta t) - \boldsymbol{u}^{v}_{mn}(t))\frac{\boldsymbol{V'}^{\boldsymbol{v}}_{mn}}{\Delta t} \quad (14)$$

The viscous strain at $t+\Delta t$ is of the form,

$$\boldsymbol{u}^{v}_{mn}(t+\Delta t) = \boldsymbol{u}^{v}_{mn}(t) + \Delta t(\boldsymbol{M}_{mn}\boldsymbol{u}_{mn} - \boldsymbol{M}^{\boldsymbol{v}}_{mn}\boldsymbol{u}^{\boldsymbol{v}}_{mn})\boldsymbol{V}^{\boldsymbol{v}}_{mn} \quad (15)$$

where the superscript v denotes the Kelvin unit, $\boldsymbol{u}^{v}_{mn}$ is the viscous deformation between nodes m and n. $\boldsymbol{V}$ and $\boldsymbol{V'}$ are symmetric matrices that include viscous force coefficients, which are proportional to the matrix $\boldsymbol{M}$. The Poisson's ratio is set to 1/4 for all components in the system in order to let the noncentral force constants equal zero, then the matrix reduces to a lower dimensionality and the system is able to be solved. $\boldsymbol{V}$ is the inverse of the matrix $\boldsymbol{V'}$. In the calculation, to avoid changing the dimensionality of force constant matrices, we can let all nonzero elements in $\boldsymbol{V}$ is the reciprocal of corresponding elements in $\boldsymbol{V'}$. In the study of stress relaxation by viscoelastic LSM, a strain is applied in the boundary and then the system equilibrated without viscous deformation. Then the viscous deformation function will run 100 iterations, and the system is relaxed to the minimum energy configuration in each iteration (Δt).

Results and discussion

A. Morphology

The microphase separations of diblock copolymer and its nanocomposites were studied by MesoDyn. An elastomeric block copolymer is considered in this work, such as thermoplastic polyurethane elastomers. This kind of polymer is composed of hard segments (H) and soft segments (S). The thermodynamic incompatibility of H and S drives the polymer system into a two-phase morphology. The incorporation of nanoparticles (N) into the elastomeric block copolymer is also performed by MesoDyn. As for thermodynamic incompatibility system, the morphology of block copolymer is strongly related to chain structures such as block sequence, block ratio, block length, and chain architecture. It means that different meso-structures can be obtained by specifying different chemical natures of the system. Bicontinuous and dispersed (hard segment disperse in soft segment matrix) structures were considered in this work.

In MesoDyn simulations, two sets of parameters should be defined: one is the chain topology in terms of repeat segments (or beads), and the other is the interaction energy between different components. Table 1 shows the Gaussian chain parameters for 12 typical polymer materials investigated in this work. Generally, two components are thermodynamically incompatible when the interaction parameter (repulsion) χ between them is larger than 0.5. The model systems here are based on PS-*b*-PAN block copolymer systems (PS: Polystyrene; PAN: Polyacrylonitrile). And the MesoDyn input parameter between H and S is 4.75. More simulation details about the structure evolution of this system can be found in Ref. [30]. The nanoparticles was simply treated as a chain with chain length of 1, and hence the distribution of nanoparticles in polymer matrix is controlled by varying the interaction parameter between nanoparticles (N) and H or S. In this work, we choose $\chi_{N,H} = 4.75$, $\chi_{N,S} = 0$ for the systems that particles selectively disperse in the soft phase ($\chi_{N,H}$ represents the interaction parameter between N and H); $\chi_{N,H} = 0$, $\chi_{N,S} = 4.75$ for the systems that particles selectively disperse in the hard phase; and $\chi_{N,H} = 4.75$, $\chi_{N,S} = 4.75$ for the systems that particles selectively disperse in the interface.

Table 1. The Gaussian chain parameters for different systems.

Polymer Materials	Gaussian Chain	Polymer Materials	Gaussian Chain
Bicontinuous Structure		Dispersed Structure	
B-1	S_{25}-H_{25}	D-1	H_5-S_{28}
B-2	S_{25}-H_{25}; N_1	D-2	H_5-S_{28}; N_1
B-3	S_{25}-H_{25}; N_1	D-3	H_5-S_{28}; N_1
B-4	S_{25}-H_{25}; N_1	D-4	H_5-S_{28}; N_1
B-5	H_{12}-S_{25}-H_{13}; N_1	D-5	S_{14}-H_5-S_{14}; N_1
B-6	H_{12}-S_{25}-H_{13}; N_1	D-6	S_{14}-H_5-S_{14}; N_1

B-1& D-1: Diblock copolymer; B-2& D-2: Diblock copolymer with nanoparticles selectively dispersed in hard phase; B-3& D-3: Diblock copolymer with nanoparticles selectively dispersed in soft phase; B-4& D-4: Diblock copolymer with nanoparticles selectively dispersed in the interface between hard and soft phases; B-5& D-5: Triblock copolymer with nanoparticles selectively dispersed in hard phase; B-6& D-6: Triblock copolymer with nanoparticles selectively dispersed in soft phase

All MesoDyn simulations were carried out in a cubic grid with 30×30×30 cells of mesh size. The grid parameter $\lambda \equiv \gamma\mu^{-1}$ =1.1543, where γ presents bond length, and μ is the mesh size. The compressibility parameter is equal to 10kT, and the total simulation time is 10000 steps without shear. The noise parameter $\Omega \equiv V^{-1}\mu^3 = 100$. The time step is 50 ns. The simulations are performed at ambient temperature 298 K. The relative concentration of nanoparticles in all systems which contain nanoparticles is equal to 2%. Note that the block copolymer is composed of hard segments and soft segments, so the relative concentration of hard or soft segments is related to the Gaussian chain topology. Table 1 shows that bead numbers of hard or soft segments in Gaussian chain are the same in all bicontinuous structure systems, it means the concentration of hard phase is equal to that of soft phase in the system.

Fig. 2 shows the dispersed morphology of different polymer materials. The system (a) without nanoparticles shows that the hard phase is spherically dispersed in the soft phase matrix. For system (b), the nanoparticles mainly concentrate in the hard phase due to the lower repulsion energy between beads N and H. In system (c) and system (d), the nanoparticles mainly concentrate in the soft phase and interface, respectively. System (e) is similar to system (b), and system (f) is similar to system (c). It can be seen that the phase domain size becomes smaller by varying the polymer chain architecture from diblock to triblock copolymer. However, the chain sequence does not impact the phase separation structure (all are dispersed morphology) in this work.

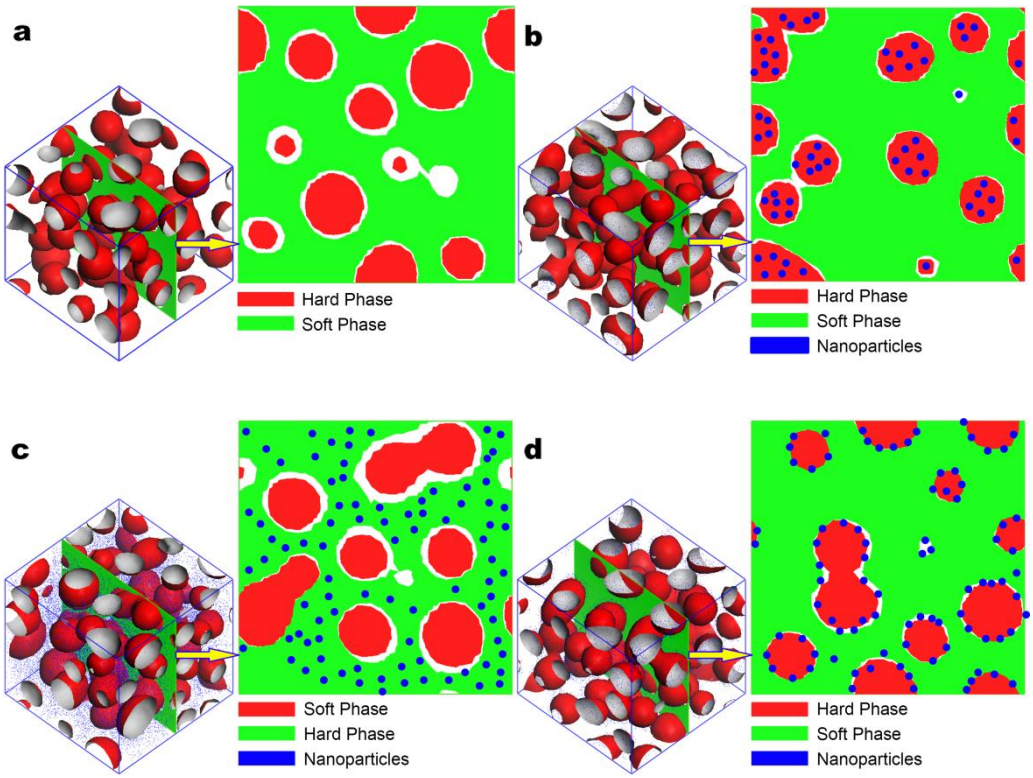

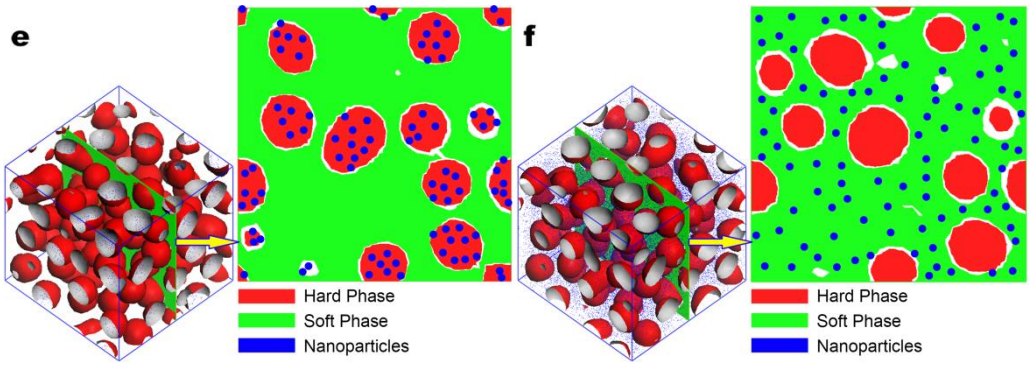

Fig. 2 Structural output (Isodensity profile of soft component and schematic model of x-y cross-section) from the MesoDyn showing typical late stage morphologies. Nanoparticles are displayed in Blue(grey) dot. The materials are (a) D-1, (b) D-2, (c) D-3, (d) D-4, (e) D-5, and (f) D-6. Schematic representation depict the distribution of nanoparticles in dispersed structures.

Interfacial area between different phases is an important parameter related to the mechanical properties. The total interfacial area is defined as $S = N_x + N_y + N_z$, where N_x, N_y and N_z are the numbers of interfacial bonds in the x, y and z directions, respectively. The total density data for each grid from the MesoDyn should be normalized to 1. Here we take two adjacent grids (Grid a and b) in the x direction for example. The influence of nanoparticles in this system is ignored due to the small amount, and the number of interfacial bonds in the x direction between grid a and b is given by

$$I_{ab} = \min\left(\rho_{PS}^{a} + \rho_{PS}^{b},\ \rho_{PP}^{a} + \rho_{PP}^{b}\right) \qquad (16)$$

where ρ_{PS}^{a} and ρ_{PP}^{a} are the densities of hard segments and soft segments in grid a, similarly, ρ_{PS}^{b} and ρ_{PP}^{b} are those in grid b, respectively. N_x are the sum of I_{ab} between all the adjacent grids in the x direction. N_y and N_z can be obtained by the same method.

Fig. 3 shows the total interfacial area of different systems when the order parameter reaches the equilibrium value. First we focus on the dispersed structures shown by orange belts (right side) in the figure. The addition of a small amount of nanoparticles has slight impact on the interfacial area, while the area increases by about 30% in triblock nanocomposites shown in the last two systems. It elucidates that the phase domain size in triblock copolymer is smaller than that in diblock copolymer. In bicontinuous structure systems, we can find a similar phenomenon that triblock nanocomposites have relatively high interfacial areas. Notably, B-2 and B-3 systems have higher interfacial areas comparing to B-1 and B-4, it means that the selective dispersal of nanoparticles in hard or soft segments narrows the phase domain size in bicontinuous structures. Actually, the incorporation of nanoparticles into polymer blends has attracted considerable attention for decades[31] because the nanoparticles can be used to control the morphology of polymer blends, [32, 33] act as the compatibilizer for immiscible polymer blends[34, 35] , e.g. the incorporation of SiO_2 in immiscible polypropylene (PP)/polyolefin elastomer (POE) blends lead to a much finer morphology[36].

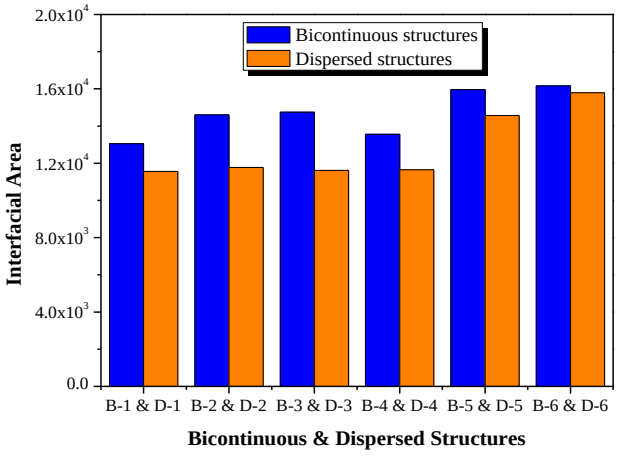

Fig. 3 Interfacial area corresponding to different composites

B. Mechanical Properties: Stiffness, Fracture Strain and Stress Relaxation

1. Young's Modulus of Elastomeric Nanocomposites

Polymer nanocomposites reinforced with low fraction of nanoparticles have received steadily growing attention owing to their unique and fascinating effect. MesoDyn simulations were carried out in a cubic grid with 30×30×30 cells of mesh size. The phase separation structures and density distribution of each cell in the cubic grid are obtained by MesoDyn. Then each cell in the grid is replaced by a node which is located in the center of the cell, the composition of each node is based on the density distribution of corresponding cell. Using the pure elastic LSM, we deform all the 12 systems along the *x* direction through the application of a strain at the system boundaries. We initially consider the elastic fields of various nanocomposites systems when the systems have been relaxed to a global strain of approximately 0.5%. The system is composed of three components, which are hard segments, soft segments, and nanoparticles. The spring constant of the hard phase, k_H, is taken to be 10 times larger than that of the soft phase, k_S, and the spring constant of nanoparticles, k_N, is 30 times larger than k_H. The spring constant is directly related to Young's modulus (elastic modulus). This disparity in elastic modulus results in complex elastic fields throughout the deformed systems. Spring constants of interfacial regions are chosen by arithmetic mean method. The total density data for each grid from the MesoDyn has been normalized to 1. Taking node *m* for example, densities of the three components are ρ_H, ρ_N and ρ_S, respectively, then the spring constant of node *m* is given by

$$k_m = \rho_H k_H + \rho_S k_S + \rho_N k_N \tag{17}$$

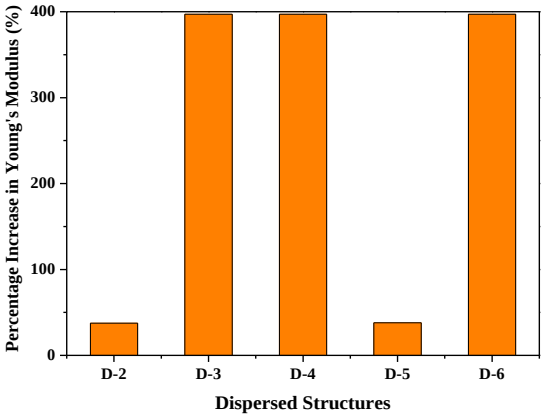

(a)

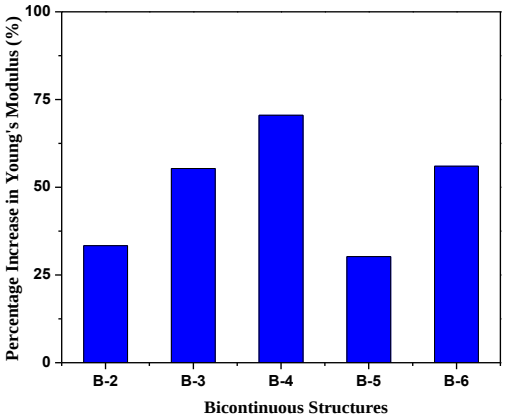

(b)

Fig. 4 The percentage increase in effective Young's modulus of different composites. (a) Dispersed systems and (b) Bicontinuous systems.

The relative concentration of nanoparticles in all nanocomposites is 2%. Note that filler loading and morphologies have strong impacts on the final mechanical responses [28, 37], the system considered in this work is treated as nanocomposites with solid spheres reinforcing nanofillers. In Fig. 4, we plot the percentage increase in Young's modulus of different polymer nanocomposites comparing to pure diblock copolymer. As shown in Fig. 4a, the dispersed structure system with nanoparticles distributed in the interface (D-4) or soft phase (D-3) has a high Young's modulus, the addition of 2% nanoparticles can make the stiffness increase about 400%. The Young's modulus of D-2 system that contains nanoparticles in hard phases increases by about 40%, which is one tenth of that in D-3 system. It proves that nanoparticles distributed in soft segments are much more efficient to enhance the stiffness than that dispersed in hard segments in dispersed structure systems. The same phenomenon can be found in D-5 and D-6 systems, for the reason that the stiffness is mainly controlled by the soft segment matrix. The Young's modulus increments in D-5 and D-6 systems are similar to those in D-2 and D-3 systems, respectively. It elucidates that reducing the phase domain size has slight influence on the percentage increase of stiffness. Fig. 4b shows the percentage increase of stiffness in bicontinuous structures. Similar to dispersed structure systems, the system with nanoparticles distributed in the interface (central column) is effective for the enhancement of Young's modulus, the stiffness increases by about 1.7 times with the addition of 2% nanoparticles. The increment of Young's modulus in B-3 system reaches to 150%, and the increment of Young's modulus in B-2 system is about 70%. The stiffness enhancement of systems with nanoparticles dispersed in soft phase (B-3 or B-6) is not as strong as that in dispersed systems (D-3 or D-6). The reason for this phenomenon is as follows. Unlike dispersed structures, the hard phase form a network in bicontinuous structures and control the stiffness, adding nanoparticles into soft phase lead to the stiffness in turn controlled by the enhanced soft phase, this will impair the enhancement efficiency in some way. In bicontinuous structures, the percentage increase in Young's modulus is comparing with the stiffness of hard segment phase instead of soft segment phase in dispersed structures. Besides, the stress concentration is easy to be alleviated by the softer phase in bicontinuous structures. From the results of B-5 and B-6 systems, reducing the phase domain size also hardly influence the enhancement of stiffness. Notably, the crystallization in polyurethane will influence the distribution of fillers in various ways due to several factors including the properties of fillers [12, 38]. But the crystallization process is related to chain structures with regular arrangement, which cannot be studied directly by the mesocopic simulation method. Similar to the Laponite reinforced polyurethane[12] where the Laponite forms a jammed structure in crystalline hard domain, the nanoparticle reinforcing effect are modeled by its density filed in LSM.

2. Fracture Strain Predicted by Pure Elastic LSM

The goal of formulating high-performance nanocomposites is not only to increase the elastic modulus but also to maintain its high extensibility (critical fracture strain). Following the calculation of stiffness, we continue to examine the extensibility of those block copolymers and their nanocomposites. In the ensuing simulations, a strain (0.5%) is applied to system boundaries and the system is equilibrated. We set the minimum fracture stress e_s closely relate to toughness of materials. Assuming that the pure diblock copolymer fracture at a global strain of 1%, and the initial time step is Δt_0, then the minimum fracture stress can be obtained. In dispersed structure systems, $e_H = 15$, $e_S = 30$; and in bicontinuous structure systems, $e_H = 25.5$, $e_S = 51$; where e_H represents the minimum fracture stress for hard phase, and e_S for soft phase. In this model, the incorporation of nanoparticles will not influence the minimum fracture stress.

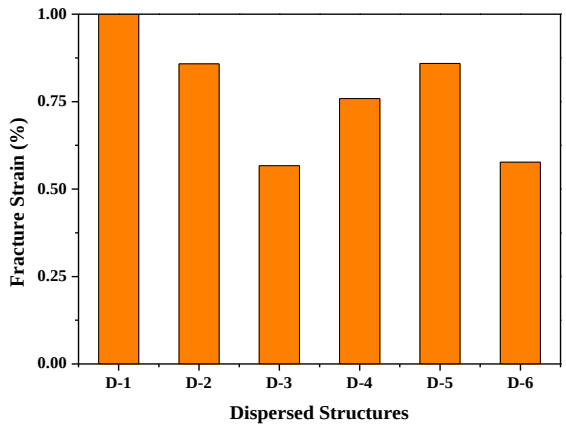

(a)

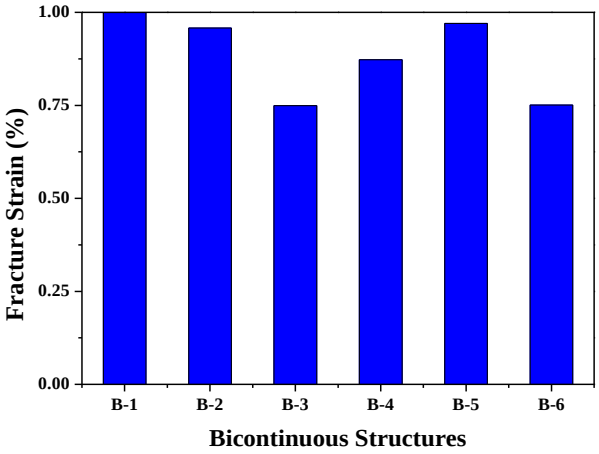

(b)

Fig. 5 The fracture strain of different polymer composites. (a) Dispersed systems and (b) Bicontinuous systems.

Fig. 5 shows the critical fracture strain of different nanocomposites with dispersed and bicontinuous structures separately. Note that the fracture strain of pure polymer system in dispersed structures (D-1) is much lower than its counterpart in bicontinuous structures (B-1) under the same situation. As can be seen in Fig. 5a, dispersing nanoparticles into hard phase (D-2 and D-5 systems) is efficient to maintain the extensibility, especially comparing to the systems with nanoparticles dispersed in soft phase (D-3 and D-6 systems). These results show a good agreement with the existing experiments[39]. By analyzing the fracture position, we find that the fracture mainly occurs in hard phase or enhanced soft phase. The extensibility is controlled by unreinforced soft segment phase in elastomeric nanocomposites, adding nanoparticles in soft segment phase will increase the total stiffness, but impair the extensibility significantly. In Fig. 5b, systems with nanoparticles dispersed in hard phase (B-2 and B-5 systems) can maintain high fracture strain (about 0.96%). While the critical fracture strain of systems with nanoparticles dispersed in soft phase (B-3 and B-6 systems) decrease by about 25%. Similarly, in polyurethane elastomer nanocomposites, nanocellulose crystals covalently bonded and specifically associated with the hard microdomains, which yields ultrahigh tensile strength and stain-to-failure[11]. Reducing phase domain size lead to a slight increase of the critical fracture strain in both bicontinuous and dispersed structure systems[29]. And the extensibility is severely impaired by the dispersal of nanoparticles in the interface (B-3 and D-3 systems). We conclude from the above analysis that adding nanoparticles in hard phase of diblock copolymer elastomers yield the stiff polymer nanocomposites with high extensibility.

3. Stress Relaxation Behavior Calculated by Viscoelastic LSM

Due to relaxation characteristics of polymer molecular movements, mechanical behaviours of polymer materials usually exhibit a combination of elastic and viscous properties. During the deformation of polymer materials, one should consider not only the applied stress or strain, but also the time for which it is applied. From the experimental aspect, the incorporation of nanofillers usually lead to the increase of viscosity and impair the stress relief. Kharchenko et al[40] reported recently a dramatic increase of the viscosity of CNT-filled polymer materials, even at low loadings. Similarly, for clay–polymer nanocomposites, the viscosity was reported to increase significantly and nonlinear viscoelastic properties were observed[41]. Using the viscoelastic LSM, we deformed the above systems through the application of a strain at the system boundaries along the *x* direction (1.5%), then the stress was relaxed and the viscous deformation function run 100 iterations, each iteration corresponded to an equilibrium state calculated by pure elastic LSM after viscous deformation. The viscosity of hard phase is 4 times greater than that of soft phase, and the viscosity of nanoparticles is 30 times greater than that of hard phase.

In order to evaluate the stress relaxation, the percentage decrease in Young's modulus is considered as a function of time in Fig. 6. The pure elastic line is obtained by pure elastic LSM for comparison. The Young's modulus for other systems deviate from the pure elastic line (straight line) due to the viscous deformation. The distribution of nanoparticles has a significant impact on the stress relaxation. Viscous deformations result in a reduction of the reinforcement efficiency. As for dispersed structures, Fig. 6a shows that the stress of diblock copolymer without nanoparticles (D-1 system) decreases by about 25% after 100 time steps, and the stress of system with nanoparticles distributed in the hard phase decreases by about 22%. However the stresses of D-3 and D-4 system decrease only by about

4% after 100 time steps. It elucidates that the viscous deformations are mainly controlled by the soft phase with the lowest viscosity, and adding nanoparticles into polymer will impair its viscosity. In Fig. 6b. The decrease amplitude of stress in bicontinuous systems is smaller than that in dispersed systems. The Young's modulus was controlled by the hard phase framework, and hence the dispersion of nanoparticles in hard phase will also impair the stress relaxation dramatically. The stress relaxation also appears to be severely impaired in systems with nanoparticles dispersed in the interphase or soft phase. In experiment, the tensile strain rate is usually quite low and the stress relaxation defers the fracture or break process. According to the time-temperature equivalence principle, the increase of relaxation time often corresponds to the increase of temperature [42].

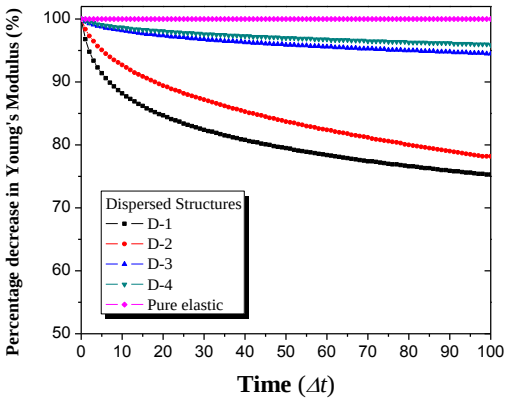

(a)

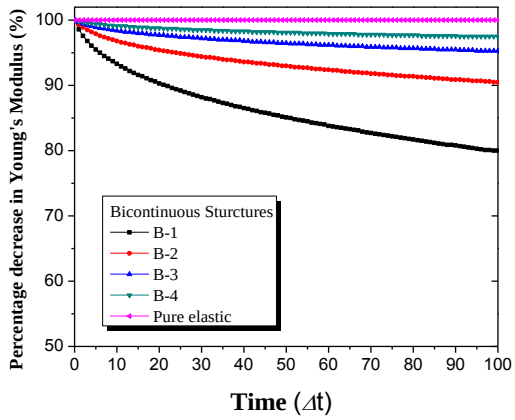

(b)

Fig. 6 The percentage increase in effective Young's modulus as a function of time for different polymer nanocomposites. (a) Dispersed systems and (b) Bicontinuous systems

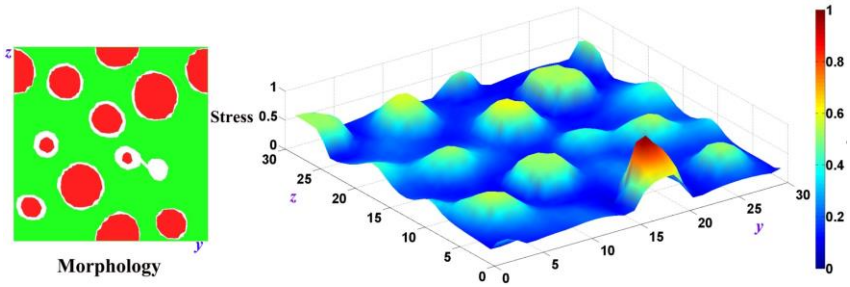

(a)

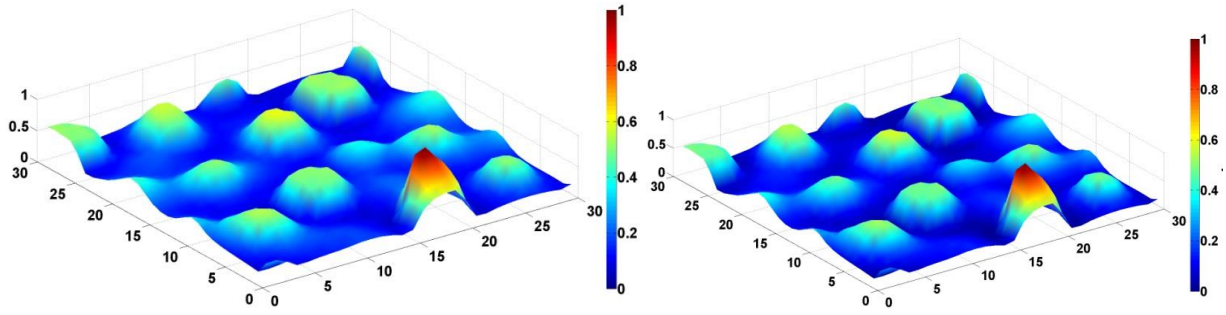

(b) (c)

Fig. 7 Normal stress fields in *z*-*y* plane ($x = x/2$) of diblock copolymer calculated by viscoelastic LSM (a) $t = 0$, (b) $t = 40\Delta t$. (c) $t = 100\Delta t$. A strain (1.5%) is applied to the system boundaries and the system is equilibrated.

In order to show the stress relaxation behavior clearly, we choose a typical system (D-1 in Fig. 6a) to show this process. Fig. 7 depicts the normal stress field for a dispersed structure diblock copolymer, where the hard phase is dispersed in soft matrix. The tensile is applied in *x* direction and the morphology are shown in the right upper corner, where the soft and hard phases are denoted with red (dark) and green (grey), respectively. It can be seen that the stress distribution is similar to the morphology, and the hard phase loads higher stress due to the larger stiffness. The viscosity of soft phase is much lower than that of hard phase. Comparing Fig. 7a with 7b, we can find a clear reduction of the average stress in soft phase after 40 time steps. With the relaxation time goes on, the stress further relaxed (Fig 7c). Note that the relaxation time considered here is not enough for the stress release in hard phase due to the high viscosity, but the average stress in hard phase is slightly reduced due to the stress transfer from the hard phase to soft phase.

Conclusions

In this paper, mesostructures of elastomeric nanocomposites and macroscospic mechanical properties were correlated by sequential mesoscopic simulation method, this method utilized MesoDyn for morphologies and LSM for mechanical responses. From the morphology result, the phase domain size became smaller by varying the polymer chain architecture from diblock to triblock copolymer. And the selective distribution of nanoparticles in hard or soft segments narrowed the phase domain size in bicontinuous structure systems[36]. The output of MesoDyn served as the input of pure elastic LSM. Simulation results showed that adding nanoparticles in polymer matrices resulted in a higher Young's modulus, and nanoparticles distributed in soft phase were more efficient to enhance the stiffness than that dispersed in hard phase. In bicontinuous structures, the hard phase formed a stiff network and controlled the stress, while in dispersed structures, the soft phase sustained the deformation and stress was hard to transfer from the soft phase to hard phase. Selective dispersion of nanoparticles in these two structures would change the stress transfer process and led to different efficiencies of stiffness enhancement. Further studies were focusing on the critical fracture strain. Adding nanoparticles in soft phase impaired the extensibility dramatically, while nanoparticles dispersed in hard phase increased the elastic modulus without loss of high extensibility. These results agreed well with experimental observations[12]. In viscoelastic LSM, our calculations showed that the viscous deformations are mainly controlled by the soft phase with the lowest viscosity and adding nanoparticles into soft segments would impair its viscosity significantly[40]. It elucidated that dispersing nanoparticles into hard phase was a reasonable way to design high-performance elastomeric nanocomposites.

Through the integration of a morphological model and a micromechanical model we have related the mechanical response of complex polymer nanocomposites without large-scale computations. The predictive capabilities of such an integrated approach can aid in the design of new materials. Rate (time)-dependent deformation behaviour is often observed in solid polymers. We have studied the stress relaxation by viscoelastic LSM, the viscous flow within the matrix was found to reduce the stress concentrations. The relation between the strain-rate and fracture process is not elucidated in this work, a feasible way is to combine probabilistic LSM and viscoelastic model, which is expected to complement more traditional mechanisms such as ductile breaking.

Acknowledgements

Financial support for this work was provided by the National Natural Science Foundation of China (No. 91334203), the 111 Project of Ministry of Education of China (Grant B08021) and the Fundamental Research Funds for the central Universities of China.

Notes and references

[a] State Key Laboratory of Chemical Engineering and Department of Chemistry, East China University of Science and Technology, Shanghai 200237, China;
[*] Fax: +86 (21) 64252921 Tel: +86 (21) 64252921. E-mail address: hlliu@ecust.edu.cn.
[b] School of Materials Science and Engineering, East China University of Science and Technology, Shanghai 200237, China

1. A. C. Balazs, T. Emrick and T. P. Russell, *Science*, 2006, **314**, 1107-1110.
2. H. Zou, S. Wu and J. Shen, *Chem. Rev*, 2008, **108**, 3893-3957.
3. C. Chevigny, N. Jouault, F. Dalmas, F. Bou é and J. Jestin, *Journal of Polymer Science Part B: Polymer Physics*, 2011, **49**, 781-791.
4. V. Baheti, J. Militky and M. Marsalkova, *Polymer Composites*, 2013, **34**, 2133-2141.
5. I. U. Unalan, G. Cerri, E. Marcuzzo, C. A. Cozzolino and S. Farris, *RSC Advances*, 2014, **4**, 29393-29428.
6. J. Zhu, M. Chen, Q. He, L. Shao, S. Wei and Z. Guo, *RSC Adv.*, 2013, **3**, 22790-22824.
7. S. Stankovich, D. A. Dikin, G. H. Dommett, K. M. Kohlhaas, E. J. Zimney, E. A. Stach, R. D. Piner, S. T. Nguyen and R. S. Ruoff, *Nature*, 2006, **442**, 282-286.
8. F. He, S. Lau, H. L. Chan and J. Fan, *Advanced Materials*, 2009, **21**, 710-715.
9. M. Moniruzzaman and K. I. Winey, *Macromolecules*, 2006, **39**, 5194-5205.
10. U. Khan, P. May, A. O'Neill, J. J. Vilatela, A. H. Windle and J. N. Coleman, *Small*, 2011, **7**, 1579-1586.
11. A. Pei, J.-M. Malho, J. Ruokolainen, Q. Zhou and L. A. Berglund, *Macromolecules*, 2011, **44**, 4422-4427.
12. S. M. Liff, N. Kumar and G. H. McKinley, *Nature materials*, 2006, **6**, 76-83.
13. T. M. Madkour, F. M. Hagag, W. Mamdouh and R. A. Azzam, *Polymer*, 2012, **53**, 5788-5797.
14. S. Deng, X. Zhao, Y. Huang, X. Han, H. Liu and Y. Hu, *Polymer*, 2011, **52**, 5681-5694.
15. X. Zhao, S. Deng, Y. Huang, H. Liu and Y. Hu, *Chinese Journal of Chemical Engineering*, 2011, **19**, 549-557.
16. B. Van Vlimmeren and J. Fraaije, *Computer physics communications*, 1996, **99**, 21-28.
17. B. Van Vlimmeren, M. Postma, P. Huetz, A. Brisson and J. Fraaije, *Physical Review E*, 1996, **54**, 5836.
18. B. Van Vlimmeren, N. Maurits, A. Zvelindovsky, G. Sevink and J. Fraaije, *Macromolecules*, 1999, **32**, 646-656.
19. K. M. Langner and G. Sevink, *Soft Matter*, 2012, **8**, 5102-5118.
20. G. Allegra, G. Raos and M. Vacatello, *Progress in Polymer Science*, 2008, **33**, 683-731.
21. R. D. Groot and P. B. Warren, *Journal of Chemical Physics*, 1997, **107**, 4423.
22. H. Chen, Y. Wu, Y. Tan, X. Li, Y. Qian and H. Xi, *European Polymer Journal*, 2012, **48**, 1892-1900.
23. G. A. Buxton, C. M. Care and D. J. Cleaver, *Modelling and simulation in materials science and engineering*, 2001, **9**, 485.
24. G. A. Buxton and A. C. Balazs, *Physical Review B*, 2004, **69**, 054101.
25. G. A. Buxton and A. C. Balazs, *Macromolecules*, 2005, **38**, 488-500.
26. L.-T. Yan, E. Maresov, G. A. Buxton and A. C. Balazs, *Soft Matter*, 2011, **7**, 595-607.
27. L. Monette, M. Anderson and G. Grest, *Polymer composites*, 1993, **14**, 101-115.
28. G. A. Buxton and A. C. Balazs, *The Journal of chemical physics*, 2002, **117**, 7649-7658.
29. S. Deng, Y. Huang, C. Lian, S. Xu, H. Liu and S. Lin, *Polymer*, 2014, **55**, 4776-4785.
30. S. Piotto, S. Concilio, F. Mavelli and P. Iannelli, in *Macromolecular symposia*, Wiley Online Library, 2009, pp. 25-33.
31. C. Huang, J. Gao, W. Yu and C. Zhou, *Macromolecules*, 2012, **45**, 8420-8429.
32. H.-j. Chung, K. Ohno, T. Fukuda and R. J. Composto, *Nano letters*, 2005, **5**, 1878-1882.
33. C. Özdilek, S. Bose, J. Leys, J. W. Seo, M. Wübbenhorst and P. Moldenaers, *Polymer*, 2011, **52**, 4480-4489.
34. T. Kwon, T. Kim, F. b. Ali, D. J. Kang, M. Yoo, J. Bang, W. Lee and B. J. Kim, *Macromolecules*, 2011, **44**, 9852-9862.
35. A. Walther, K. Matussek and A. H. Muller, *Acs Nano*, 2008, **2**, 1167-1178.
36. S. H. Lee, M. Kontopoulou and C. B. Park, *Polymer*, 2010, **51**, 1147-1155.
37. H. Kausch and G. Michler, *Journal of applied polymer science*, 2007, **105**, 2577-2587.
38. B. Fernández-d'Arlas, U. Khan, L. Rueda, J. N. Coleman, I. Mondragon, M. A. Corcuera and A. Eceiza, *Composites Science and Technology*, 2011, **71**, 1030-1038.
39. L. T. James Korley, S. M. Liff, N. Kumar, G. H. McKinley and P. T. Hammond, *Macromolecules*, 2006, **39**, 7030-7036.

40. S. B. Kharchenko, J. F. Douglas, J. Obrzut, E. A. Grulke and K. B. Migler, *Nature materials*, 2004, **3**, 564-568.

41. J. Ren and R. Krishnamoorti, *Macromolecules*, 2003, **36**, 4443-4451.

42. Y. M. Boiko, W. Brostow, A. Y. Goldman and A. Ramamurthy, *Polymer*, 1995, **36**, 1383-1392.